CHEMISTRY OF MATERIALS

pubs.acs.org/cm

Article

Exploring the Links between Photoluminescence and Microstructure in $Cs_2InBr_5{\cdot}H_2O$ Samples Doped with Pb^{2+}

Jackson D. Majher, Victor da Cruz Pinha Barbosa, Chris Chae, T. Amanda Strom, Jinwoo Hwang, and Patrick M. Woodward*

Cite This: *Chem. Mater.* 2023, 35, 482–489

Read Online

ACCESS | Metrics & More | Article Recommendations | Supporting Information

ABSTRACT: Precipitation of $Cs_2InBr_5{\cdot}H_2O$ from HBr(aq) solutions containing Pb^{2+} ions results in powders that exhibit narrowband green photoluminescence (λ_{max} = 521 nm, fwhm = 89.9 meV). Synchrotron powder X-ray diffraction reveals trace amounts of Cs_4PbBr_6 and $CsPbBr_3$ that cannot be detected by laboratory powder diffraction measurements. Broadening of the $CsPbBr_3$ diffraction peaks suggests crystals that are tens of nanometers in size. Evidence for the presence of $CsPbBr_3$ can also be seen in diffuse reflectance spectra. Cathodoluminescence imaging shows that luminescence originates from small nanometer-sized regions. Taken together, these observations point to $CsPbBr_3$ nanocrystal inclusions as the source of photoluminescence. Heating these samples to temperatures at or above 80 °C triggers a reversible dehydration process that leads to an irreversible change in the photoluminescence from green to blue ($\lambda_{max} \approx$ 480 nm, fwhm = 278 meV), accompanied by significant changes in the microstructure. Cathodoluminescence imaging indicates that the blue emission occurs over much larger micron-sized regions of the sample. The position of blue PL is similar to other hybrid lead bromide compounds where the emission has been assigned to $^3P_1 \rightarrow {}^1S_0$ transitions on $[PbBr_4]^{2-}$ ions. Based on the emission wavelength and cathodoluminescence imaging, the blue emission is assigned to isolated $[PbBr_4]^{2-}$ ions that substitute for $[InBr_5{\cdot}H_2O]^{2-}$ ions in the parent hydrate phase. This work provides new insight on the spontaneous formation of halide perovskite nanocrystals in an inert matrix, one that does not rely on the use of organic solvents and is stable in ambient atmospheres.

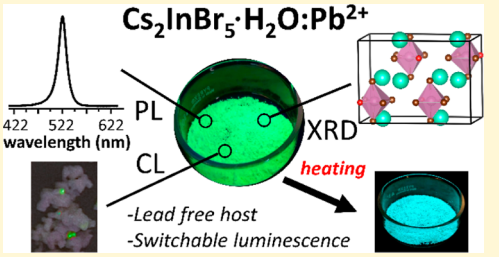

INTRODUCTION

Halide perovskites with formula ABX_3 (A = Cs^+, $CH_3NH_3^+$, $NH_2CHNH_2^+$; B = Pb^{2+}; X = Cl^-, Br^-, I^-) have received considerable attention for their optoelectronic properties. Favorable characteristics include long diffusion lengths, high absorption coefficients, and chemical tunability.[1−3] Perovskite nanocrystals (NC) have also been extensively studied, motivated in large part by their highly efficient narrowband photoluminescence (PL) that can be compositionally tuned across the visible range.[4−6] The luminescence behavior of perovskite NCs has potential for use in a variety of applications including light emitting diodes (LEDs), scintillators, lasers, photodetectors, and quantum computing.[7−10] Despite their favorable optoelectronic properties, applications of halide perovskites are ultimately limited by the presence of Pb^{2+}, an ion that is well documented to have a variety of adverse health effects.

To help circumvent these issues, lead-free analogues of the halide perovskite structure have been explored. Halide double perovskites with formula $A_2BB'X_6$ (A = Cs^+; B = Ag^+, Na^+; B′ = Bi^{3+}, In^{3+}; X = Cl^-, Br^-) have a similar structure to lead-based perovskites but eliminate Pb^{2+} by replacing it with equal proportions of 1+ and 3+ ions.[11−13] Various strategies have been used to enhance the PL properties of these materials including doping with transition metal and rare earth activator ions, symmetry-breaking to enhance self-trapped exciton emission, and doping with ns^2 activator ions.[14−22] Doping with ns^2 activators (Sb^{3+}, Bi^{3+}, etc.) has led to efficient photoluminescent systems due to localized absorption and emission from the activator site, as exemplified by $Cs_2NaInCl_6:Sb^{3+}$ which exhibits strong blue PL.[19−21] Other photoluminescent lead-free perovskite derivatives that have been developed include perovskite related phases such as $Cs_2SnCl_6/M^{3+/4+}$ (M = Bi^{3+}, Sb^{3+}, Te^{4+}), and $Rb_3InCl_6:Sb^{3+}$, as well as several hydrate phases with formula $A_2InX_5{\cdot}H_2O:Sb^{3+}$ (A = Cs^+, Rb^+; X = Cl^-, Br^-).[23−30]

Sb^{3+}-doped hydrate phases have drawn significant interest due to their ease of synthesis, high quantum yield, and tunable PL. $Cs_2InCl_5{\cdot}H_2O:Sb^{3+}$ has been prepared with PL quantum yield (PLQY) reaching an impressive 95.5% and emission that can be tuned from 580 to 660 nm through Br^-/I^- substitution.[29] By monitoring the change in PL triggered by dehydration, $Cs_2InBr_5{\cdot}H_2O:Sb^{3+}$ has been shown to act as a

Received: September 13, 2022
Revised: December 20, 2022
Published: January 3, 2023

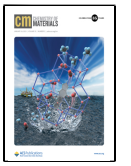

sensitive moisture detector.[30,31] These phosphors have also demonstrated potential for phosphor-converted LEDs and high-resolution fluorescence imaging applications.[29]

Although many ns^2 ion dopants have been applied to enhance the PL properties of halide materials, there are relatively few studies of Pb^{2+} activators in halide perovskite hosts. Recently, Cs_4PbBr_6, with isolated Pb-centered octahedra, has garnered significant interest due to its narrowband green emission. The origin of this luminescence is thought to arise from $CsPbBr_3$ NC inclusions that form spontaneously in the structure.[32,33] The Cs_4PbBr_6 host structure encapsulates $CsPbBr_3$ NCs and improves their stability under ambient conditions. However, the presence of Pb^{2+} in the host structure offers no relief from toxicity concerns associated with competing Pb-based halide perovskites.

Here, we report the synthesis and characterization of $Cs_2InBr_5{\cdot}H_2O$ samples that have been precipitated from HBr(aq) solutions containing Pb^{2+} ions. Samples synthesized at low temperature exhibit narrowband green emission that is characteristic of $CsPbBr_3$ NC. Synchrotron powder X-ray diffraction (PXRD) analysis provides evidence for the presence of $CsPbBr_3$ in green emitting samples. Heating these samples to induce dehydration initiates a change in the microstructure and changes the PL from green to blue, a feature not before observed in Cs_4PbBr_6 hosts or any other material containing perovskite NC. The blue emission is attributed to isolated Pb^{2+} ions that substitute for In^{3+} in the $Cs_2InBr_5{\cdot}H_2O$ host crystal. Cathodoluminescence (CL) measurements provide further evidence to support the origins of green and blue PL.

EXPERIMENTAL SECTION

CsBr (Alfa Aesar, 99%), In_2O_3 (Alfa Aesar, 99.994%), $InBr_3$ (Fisher Scientific, 99.99%), $PbBr_2$ (Alfa Aesar, 98+%), Sb_2O_3 (Acros Organics, 99+%), HBr (Sigma-Aldrich, 40 wt % in H_2O), dimethyl sulfoxide (DMSO) (Fisher Scientific, 99.6%), and diethyl ether (Fisher Scientific, 99%) were all used as received.

The synthesis of undoped $Cs_2InBr_5{\cdot}H_2O$ was carried out using conditions similar to those reported in ref 29. First, In_2O_3 (2 mmol) was added to HBr (20 mL, 60 °C) and stirred until the solution was clear. CsBr (8 mmol) was then added, triggering precipitation of the product. The solution was allowed to stir for another hour and then separated from the solution via vacuum filtration through a fritted funnel. The precipitate was washed with diethyl ether during filtration to promote drying. The product thus obtained was a white powder that was stored under ambient conditions. Samples of $Cs_2InBr_5{\cdot}H_2O/Sb^{3+}$ were prepared in the same manner, but Sb_2O_3 (0.2 mmol) dissolved in solution before addition of CsBr. The resulting product was a white powder that exhibited orange PL.

Samples of $Cs_2InBr_5{\cdot}H_2O{:}Pb^{2+}$ that exhibited green PL were synthesized as follows. First, In_2O_3 (2 mmol) and a variable amount of $PbBr_2$ (0.4−2 mmol) were dissolved in hydrobromic acid (20 mL, room temperature) and stirred until the solution was clear. The flask was then placed in an ice bath and stirred for 15 min. CsBr (8 mmol) was then added to trigger the precipitation of the product. The solution was monitored with a 365 nm UV flashlight until the emergence of green PL was observed. This typically occurred approximately 10 min after CsBr addition. The solution was stirred for an additional hour and then separated from the solvent via vacuum filtration through a fritted funnel. While on the vacuum line, the powder was washed twice with fresh HBr, left for 30 min, and then washed with diethyl ether. If the sample is not washed with fresh HBr an orange powder formed upon diethyl ether washing. Apparently, this step helps wash away excess Pb^{2+} ions.

Two methods were used to obtain $Cs_2InBr_5{\cdot}H_2O{:}Pb^{2+}$ samples that exhibited blue PL. One approach was to prepare $Cs_2InBr_5{\cdot}H_2O{:}Pb^{2+}$ with green PL as described above, but before filtration, the flask was transferred to an oil bath and heated at 80 °C for 2−12 h. After this "annealing" step, the powder was isolated from the solution by filtration. An alternative approach was to heat dry $Cs_2InBr_5{\cdot}H_2O{:}Pb^{2+}$ powders to 80 °C for 10 h and then cool back to room temperature.

The synthesis of Cs_4PbBr_6 was carried out as follows. First, $PbBr_2$ (3.5 mmol) was dissolved in 10 mL of DMSO. In a separate vessel, CsBr (7 mmol) was dissolved in 5 mL of HBr. The CsBr solution was then added dropwise to the solution containing $PbBr_2$ leading to precipitation of the product. The solution was stirred for several hours and then filtered via vacuum filtration in a fritted funnel. The product was washed with ethanol and isolated as a yellow powder with green PL.

PXRD data were collected on a Bruker D8 ADVANCE powder diffractometer (40 kV, 40 mA, sealed Cu X-ray tube) equipped with an incident beam monochromator (Johansson type SiO_2 crystal) that selects only Cu Kα1 radiation (λ = 1.5406 Å) and a Lynxeye XE-T position-sensitive detector. Synchrotron PXRD was collected on the 11-BM beamline at the advanced photon source (APS). Samples were packed into 0.8 mm Kapton tubes and sealed with clay. Rietveld refinements of laboratory PXRD data were carried out using the TOPAS-Academic (Version 6) software package to determine the crystal structure.[34] Crystal structure images were generated with Vesta 3.[35]

UV−vis diffuse reflectance spectra were obtained with a PerkinElmer Lambda 950 spectrometer with a 60 mm InGaAs integrating sphere. Steady-state PL data were obtained using a Jovin Horiba FluoroMax4 (Xenon source, 3 nm excitation and emission slit widths, 1 nm step size) equipped with a solid-state sample holder and R928 PMT detector. Luminescent data were analyzed using the FluorEssence (v3.5) software powered by Origin. Internal photoluminescent quantum yield (PLQY) measurements were performed with a Jovin Horiba FluoroMax4 equipped with a Quanta-φ integrating sphere (15 cm) and a PTFE sample cup with a fused quartz cover slip. An equivalent volume of non-luminescing barium sulfate was used as the blank reference sample. Radiometric, sphere, and dark count corrections were applied during data acquisition, while corrections for filters and integration time differences were applied in the FluorEssence analysis package for Quantum Yield (FluorEssence v3.8.0.60, Origin v8.6001). Additional details are available in the Supporting Information.

Thermogravimetric analysis (TGA) was performed on a Thermogravimetric Analyzer TGA Q50. Samples were heated under a nitrogen stream of 50 mL/min with a heating rate of 10 °C/min between 25 and 800 °C.

Scanning electron microscopy (SEM) images were obtained by using a Themo Scientific Apreo FEG SEM. The microscope is equipped with a retractable CL detector for direct imaging of red, blue, or green light generated when the samples are exposed to the high energy electrons. The microscope operated in low vacuum mode, where water vapor is added to partially neutralize the electron beam since the sample is non-conducting. The micrographs were taken at an accelerating voltage of 20 kV and a current of 1.6 nA.

RESULTS

$Cs_2InBr_5{\cdot}H_2O$ is isostructural to a large family of metal halide hydrates with the general formula $A_2MX_5{\cdot}H_2O$ (A = Cs^+, Rb^+, K^+; M = In^{3+}, Tl^{3+}, Y^{3+}, Sc^{3+}, Fe^{3+}; X = Cl^-, Br^-). The structure is composed of isolated $[InBr_5(H_2O)]^{2-}$ octahedra separated by Cs^+ ions. The cesium cation is coordinated by 10 bromide ions. The In−Br bonds are all fairly similar in length (~2.61−2.66 Å), and the In−OH_2 distance is shorter (~2.37 Å) resulting in a distorted octahedral environment. The crystal structure is similar to a vacancy ordered perovskite, A_2MX_6 (e.g., Cs_2SnBr_6), where the oxidation state of the B-site is reduced from +4 to +3, and a Br^- ion is replaced by a neutral H_2O ligand (Figure S1). Synchrotron PXRD was used to confirm the purity of synthesized samples, and Rietveld refinement confirmed the compound crystallizes in the *Pnma*

https://doi.org/10.1021/acs.chemmater.2c02817
Chem. Mater. 2023, 35, 482−489

space group with refined lattice parameters a = 14.95285(2) Å, b = 10.90493(2) Å, c = 7.70033(1) Å (Figures 1 and S2) in close agreement to those found in the literature.[31]

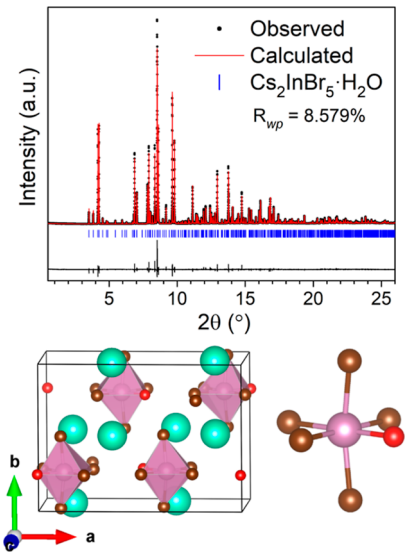

Figure 1. Top: Rietveld fit of undoped $Cs_2InBr_5{\cdot}H_2O$. Synchrotron diffraction data taken on beamline 11-BM (λ = 0.458162 Å) at the APS. Observed data are given in black, Rietveld fit is given in red, allowed peak positions for $Cs_2InBr_5{\cdot}H_2O$ (*Pnma*) are indicated with blue tick marks. The difference between observed and calculated patterns is represented by the black curve at the bottom. Bottom: unit cell and a view of the $[InBr_5(H_2O)]^{2-}$ complex ion. The In^{3+} cation is shown in purple, Cs^+ in cyan, Br^- in brown, and O^{2-} in red.

The addition of $PbBr_2$ to solution before triggering precipitation was found to produce a product which exhibits either green or blue PL depending upon details of the synthetic procedure. Figure 2 depicts the synthetic routes that lead to

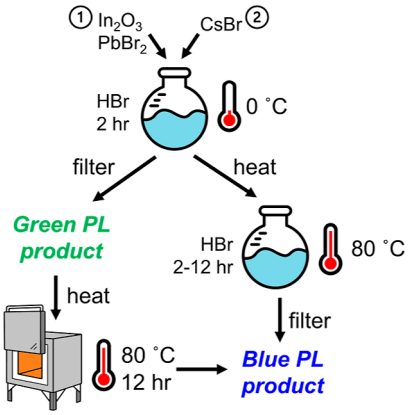

Figure 2. Synthetic routes to either green emitting or blue emitting $Cs_2InBr_5{\cdot}H_2O{:}Pb^{2+}$. Additional details are provided in the experimental section.

Pb^{2+}-doped $Cs_2InBr_5{\cdot}H_2O$ samples with either green or blue PL. Interestingly, it was found that lowering the synthesis temperature, such as doing the reaction in an ice bath, favored the formation of product with narrowband green luminescence. If the precipitation step was initiated at higher temperatures (e.g., 80 °C), the product would exhibit weak or no luminescence.

Laboratory PXRD was not able to resolve any differences between the diffraction patterns of undoped $Cs_2InBr_5{\cdot}H_2O$ and samples doped with Pb^{2+} that exhibited either green or blue PL (Figure S3). However, analyzing samples of $Cs_2InBr_5{\cdot}H_2O{:}Pb^{2+}$ with green PL via high resolution synchrotron PXRD revealed small quantities of Cs_4PbBr_6 (1.2% by mass) and CsBr (0.7% by mass) as determined through Rietveld refinements (Figures 3, S4 and S5). Furthermore, the presence

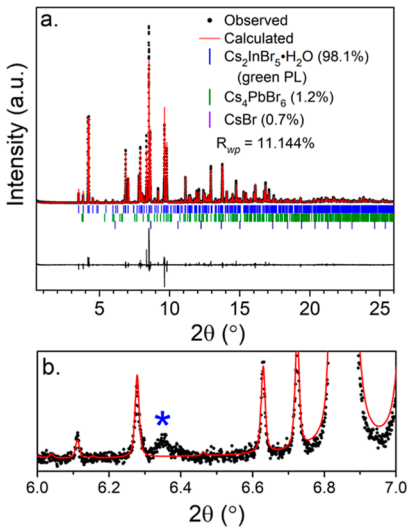

Figure 3. (a) Rietveld fit of $Cs_2InBr_5{\cdot}H_2O{:}Pb^{2+}$ exhibiting green PL. Synchrotron diffraction data taken on beamline 11-BM (λ = 0.458162 Å) at the APS. Refined phases include $Cs_2InBr_5{\cdot}H_2O$, Cs_4PbBr_6, and CsBr. Experimental data are shown with black points, the calculated pattern in red, and allowed peak positions for $Cs_2InBr_5{\cdot}H_2O$ (*Pnma*) are denoted with blue, Cs_4PbBr_6 ($R\bar{3}c$) green, and CsBr ($Pm\bar{3}m$) purple tick marks. The difference between observed and calculated patterns is given below in black. (b) Zoomed in region of the top figure. The blue asterisk denotes a peak that is tentatively assigned to $CsPbBr_3$, as discussed in the text.

of $CsPbBr_3$ was signaled by a weak, broad peak positioned at ~6.3° 2θ, which is the expected position of the overlapping (121), (200), and (002) reflections of the orthorhombic structure of $CsPbBr_3$. In the PXRD pattern of bulk $CsPbBr_3$, these overlapping peaks together constitute the strongest reflection in the pattern, so their presence here is taken as evidence for $CsPbBr_3$. This peak is considerably broader than those around it, suggesting size broadening due to small crystallite size (Figure 3). Neglecting the very subtle splitting of the three peaks (the orthorhombic structure of $CsPbBr_3$ is highly pseudocubic) Scherrer analysis of the peak width suggests a crystallite size of approximately 30 nm, comparable to what has been found previously in green-emissive Cs_4PbBr_6 phases (Figures S6 and S7).[36]

Absorption spectra were approximated by applying a Kubelka–Munk transformation to diffuse reflectance measurements on powder samples. Undoped $Cs_2InBr_5{\cdot}H_2O$ has an absorption onset at 3.86 eV (321 nm), consistent with prior reports.[31] Samples doped with Pb^{2+} exhibit an absorption tail that extends well below the band edge of undoped $Cs_2InBr_5{\cdot}H_2O$. The onset of absorption for the sub-band gap feature was determined to be 2.33 eV (532 nm), a value similar to the onset reported for $CsPbBr_3$ NCs (Figure S8).[37] Excitation measurements show a maximum at 3.43 eV (361 nm), but excitation extends well into the visible region and continues

https://doi.org/10.1021/acs.chemmater.2c02817
Chem. Mater. 2023, 35, 482−489

out to wavelengths approaching the emission peak. Narrowband emission of green light occurs with λ_{max} = 521 nm and fwhm = 89.9 meV (19.8 nm) (Figures 4 and S9). The samples

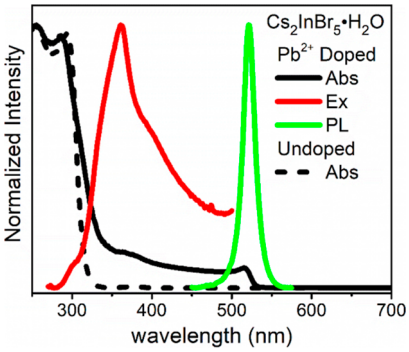

Figure 4. Absorption, excitation, and PL spectra of $Cs_2InBr_5{\cdot}H_2O{:}Pb^{2+}$ with green PL. Absorption of undoped $Cs_2InBr_5{\cdot}H_2O$ is given by the dashed line.

with the highest PLQY (7%) were obtained when 0.15 mol $PbBr_2$ per mole of $Cs_2InBr_5{\cdot}H_2O$ was added to the solution (Figure S10). The optical properties of $Cs_2InBr_5{\cdot}H_2O{:}Pb^{2+}$ samples exhibiting green PL are compared to those of Cs_4PbBr_6 in the Supporting Information (Figures S11−S14). The weak sub-band gap absorption characteristics, narrowband green emission, and small Stokes shift are very similar in both materials, suggesting the luminescence in $Cs_2InBr_5{\cdot}H_2O{:}Pb^{2+}$ comes from $CsPbBr_3$ NCs.

Samples exhibiting green PL are stable under ambient conditions indefinitely, with no change in PL observed after several months (Figure S15). However, heating these dry, powder samples in air or vacuum to 80 °C for 10 h results in an irreversible shift from green to blue emission. Blue PL may be also be achieved by heating freshly precipitated $Cs_2InBr_5{\cdot}H_2O{:}Pb^{2+}$ to 80 °C while still in solution prior to filtration and washing (Figure 2). Synchrotron PXRD analysis of samples prepared by the solution route reveals only $Cs_2InBr_5{\cdot}H_2O$, with no sign of the secondary phases Cs_4PbBr_6, CsBr, or $CsPbBr_3$ (Figures 5 and S16). The presence of blue PL in samples containing only $Cs_2InBr_5{\cdot}H_2O$ strongly suggests that PL is coming from that phase and not from embedded $CsPbBr_3$ NCs. A similar analysis of $Cs_2InBr_5{\cdot}H_2O{:}Pb^{2+}$ samples where

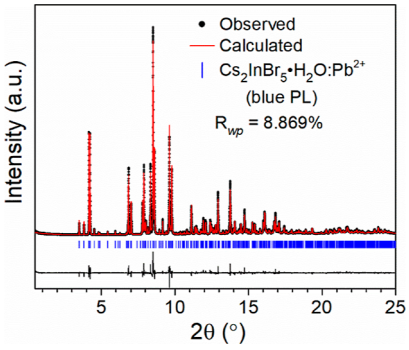

Figure 5. Rietveld fit of $Cs_2InBr_5{\cdot}H_2O{:}Pb^{2+}$ exhibiting blue PL. Synchrotron diffraction data taken on beamline 11-BM (λ = 0.458162 Å) at the APS. Collected data are given in black, Rietveld fit is given in red, expected peak positions for $Cs_2InBr_5{\cdot}H_2O$ (*Pnma*) are denoted with blue tick marks. The difference between the observed data and the fit is given below in black.

blue PL is obtained by heating to 80 °C post-synthesis shows a reduction of the intensities of peaks associated with Cs_4PbBr_6 and accompanied by an increase in intensity and narrowing of the XRD peak associated with $CsPbBr_3$ (Figure S17). This change indicates a growth in particle size of the $CsPbBr_3$ phase upon heating and may explain the slight orange discoloration seen in these samples. This would seem to suggest that the $CsPbBr_3$ NCs are expelled from the $Cs_2InBr_5{\cdot}H_2O$ matrix and coalesce into crystals too large to show PL at room temperature.

The blue emission is centered at 480 nm with a larger fwhm of 278.5 meV (Figures 6 and S18). The PLQY for the

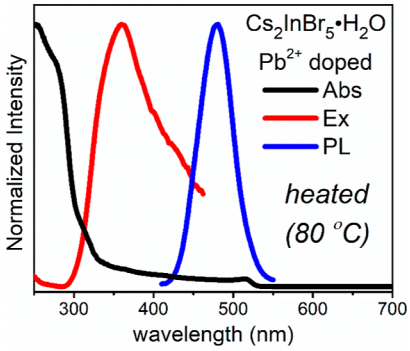

Figure 6. Absorption, excitation, and PL spectra of $Cs_2InBr_5{\cdot}H_2O{:}Pb^{2+}$ with blue PL. This sample was heat-treated at 80 °C for 10 h post-synthesis.

$Cs_2InBr_5{\cdot}H_2O{:}Pb^{2+}$ sample prepared from a solution that had been heated to 80 °C was measured to be 41%, significantly higher than that measured for green emitting samples and also higher than a blue emitting $Cs_2InBr_5{\cdot}H_2O{:}Pb^{2+}$ sample heated post-synthesis, which had a PLQY of 16%. No significant change is observed in the absorption or excitation features of the phosphor and the sub-band gap absorption feature remains regardless of the synthesis route. Unlike the green emission, the emission profile of blue PL $Cs_2InBr_5{\cdot}H_2O{:}Pb^{2+}$ is not stable and gradually shifts to longer wavelengths over time (Figure 7). For samples heated post-synthesis, this redshift happens slowly whereas when heated in solution, this process happens more rapidly with full conversion happening over the course of 12 h (Figure 7). Despite the redshift of the emission, there was no observation of complete conversion back to the green PL product. Re-heating the samples to around 80 °C did not return the emission peak back to 480 nm but instead seemed to accelerate the shifting to its new position at 510 nm. Heating either green PL or blue PL to higher temperatures (300 °C) leads to an orange coloration of the powder, suggestive of bulk $CsPbBr_3$ formation, and loss of luminescence (Figure 8). CIE coordinates of the green PL product and blue PL products are provided in the Supporting Information.

To probe the cause of the PL change, TGA measurements were taken to monitor any decomposition of the sample in this temperature range. TGA shows an initial 2.5% weight loss starting at approximately 100 °C, which is in close agreement to the theoretical mass percent of H_2O in the sample of 2.3%, indicating a dehydration mechanism upon heating. Further decomposition is not observed until 450 °C. Because conversion from the green to blue PL product occurs at 80 °C, seemingly below the dehydration temperature; further measurements were carried out at this temperature to probe

https://doi.org/10.1021/acs.chemmater.2c02817
Chem. Mater. 2023, 35, 482−489

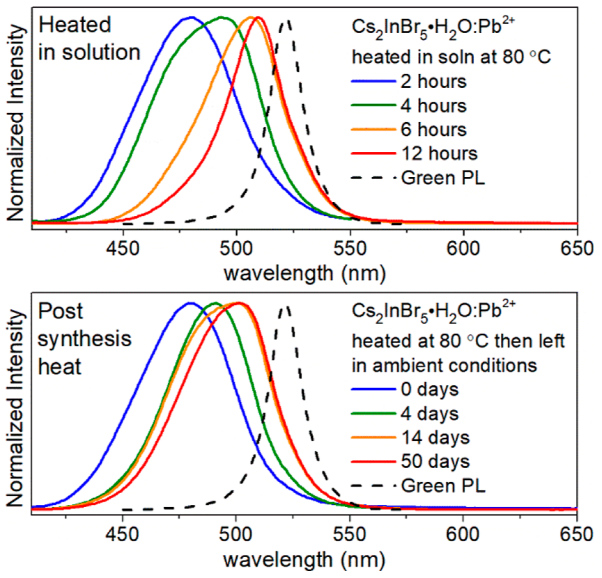

Figure 7. Evolution of PL in blue emitting $Cs_2InBr_5{\cdot}H_2O$:Pb^{2+} samples as a function of time. The top figure is for samples that were heated in solution for varying amounts of time, then removed from solution, and PL was measured. The bottom figure is for a sample left under ambient conditions with periodic PL measurements. The PL of a green emitting $Cs_2InBr_5{\cdot}H_2O$:Pb^{2+} sample (dashed line) is included to show that PL does not fully return to its original state.

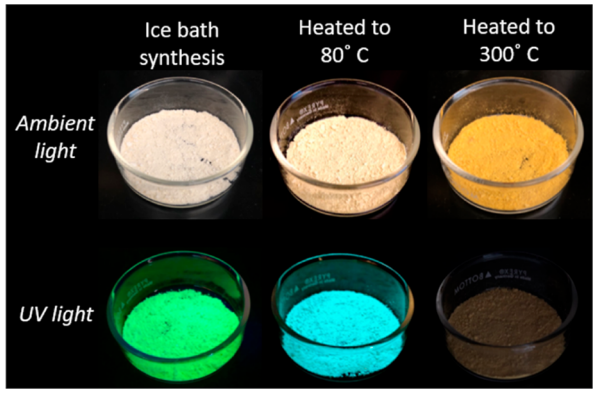

Figure 8. Sample appearance under ambient light and UV light after being synthesized and heated to various temperatures. Pictures were taken after each sample cooled down to room temperature.

stability. In fact, holding the sample at 80 °C is sufficient to trigger the dehydration of the product over a period of 4.5 h (Figure 9). Thus, the dehydration/rehydration process of $Cs_2InBr_5{\cdot}H_2O$ is closely linked to the transformation from green PL to blue PL.

Next, we turned to CL imaging to better understand the spatial distribution of PL. As seen in Figure 10, emission in green PL samples is localized to very small regions of the sample. This is consistent with CL measured on Cs_4PbBr_6 samples where PL is thought to occur from $CsPbBr_3$ NC.[38] Interestingly, the CL profile of blue PL samples is strikingly different. It is more diffusive and originates from much larger micron-sized regions of the sample. SEM images also show that the dehydration/rehydration process leads to significant growth in grain size.

As a comparison, CL analysis was carried out on $Cs_2InBr_5{\cdot}H_2O$ samples doped with Sb^{3+}. Luminescence in this system is

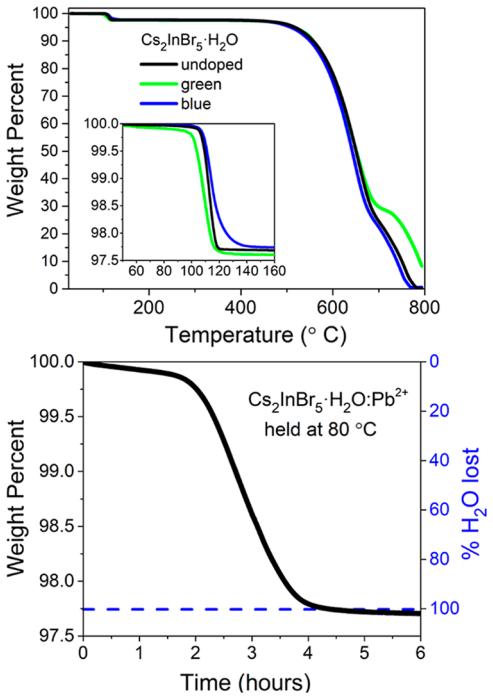

Figure 9. Top: TGA of undoped and Pb^{2+}-doped $Cs_2InBr_5{\cdot}H_2O$ samples highlighting the region near 100 °C where the material loses water. Bottom: TGA of sample held at 80 °C for 6 h showing the loss of water as a function of time.

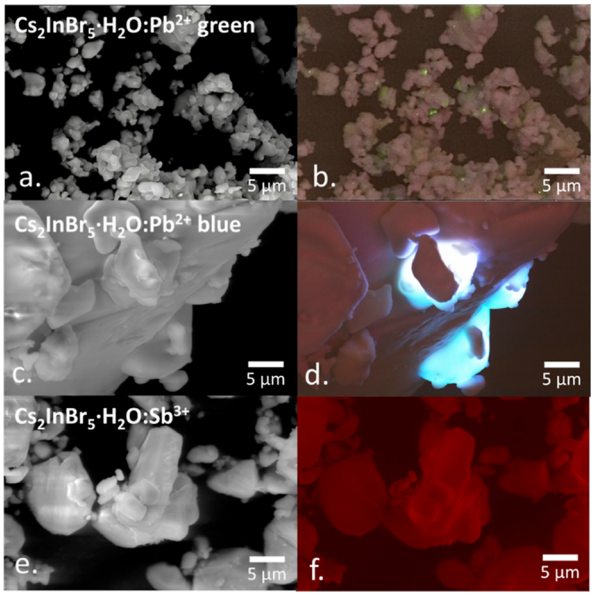

Figure 10. (a) SEM and (b) CL of green emitting $Cs_2InBr_5{\cdot}H_2O$:Pb^{2+}; (c) SEM and (d) CL of blue emitting $Cs_2InBr_5{\cdot}H_2O$:Pb^{2+}; (e) SEM and (f) CL of orange emitting $Cs_2InBr_5{\cdot}H_2O$:Sb^{3+}. Additional images are provided in the Supporting Information.

understood to arise from a simple Sb_{In} substitution mechanism yielding orange-red emission.[29,30] Figure 10 shows that the spatial variations in CL intensity are visually similar to blue PL, as seen in Pb^{2+} doped samples, suggesting that the blue PL arises from isolated Pb^{2+} dopants rather than localized $CsPbBr_3$ NC. An alternative explanation for the blueshifted PL could be the shrinking of NC domains in the green PL samples, leading to increased quantum confinement effects and a blueshift of

https://doi.org/10.1021/acs.chemmater.2c02817
Chem. Mater. 2023, 35, 482−489

the emission peak. However, CL and synchrotron PXRD provide evidence that directly contradicts this hypothesis. In fact, the breadth and peak position of blue PL samples is remarkedly similar to that reported for $Bmpip_2PbBr_4$, a hybrid material possessing isolated $PbBr_4^{2-}$ ions with Pb^{2+} in disphenoidal (seesaw) coordination.[39]

DISCUSSION

The characteristics of the excitation and emission bands, the presence of a broad peak associated with $CsPbBr_3$ in the synchrotron PXRD pattern, and the localized emission seen in the CL all point toward the green PL seen in these samples as originating from $CsPbBr_3$ NC. Given the available data, we cannot conclusively determine if the $CsPbBr_3$ NC are embedded in the hydrate phase itself or within Cs_4PbBr_6 crystals that make up 1−2% of the sample. Diffuse reflectance spectra show similar intensity of the sub-band gap absorption attributed to $CsPbBr_3$ in both $Cs_2InBr_5{\cdot}H_2O{:}Pb^{2+}$ and Cs_4PbBr_6 samples, yet the strong Cs_4PbBr_6 absorption band is not detected in the former (Figure S12). This observation suggests that $CsPbBr_3$ NC can be stabilized in a $Cs_2InBr_5{\cdot}H_2O$ matrix and do not need to be surrounded by Cs_4PbBr_6.

The synthesis of the green emitting phosphors studied here differs in important ways from other routes to $CsPbBr_3$ NC. The formation of $CsPbBr_3$ NC consists of a hot injection method consisting of rapid addition of Cs^+ to a solution of PbX_2 salts in a nonpolar solvent at high temperatures (140−200 °C) under an inert atmosphere. Alternatively, perovskite nanowires have been grown using a ligand-assisted reprecipitation method at ice bath temperatures in anhydrous solvents such as dimethylformamide (DMF) and toluene.[40] A $CsPbBr_3$ NC encapsulated in a Cs_4PbBr_6 host is prepared by combining the halide salts in a mixture of DMF and DMSO. To the best of our knowledge, there are no reported syntheses of green emitting Cs_4PbBr_6 samples without the addition of DMF or DMSO. The switch to precipitation from an aqueous solution reported here offers a more facile and environmentally friendly synthesis route.

The PL changes from green to blue upon heating samples to a sufficiently high temperature to induce dehydration. This is accompanied by a reduction in the intensity of Cs_4PbBr_6 PXRD peaks and a significant sharpening of the $CsPbBr_3$ diffraction peaks. The latter observation is consistent with the presence of larger $CsPbBr_3$ crystallites. SEM images also show significant grain growth of the main $Cs_2InBr_5{\cdot}H_2O$ crystallites. Upon dehydration, $Cs_2InBr_5{\cdot}H_2O$ is reported to undergo a phase change to a mixture of $Cs_3In_2Br_9$ and CsBr.[31] Based on our studies, when cooled back to room temperature and exposed to air, the material rehydrates in a matter of minutes, reforming the $Cs_2InBr_5{\cdot}H_2O$ phase. The transformation of the hydrate phase to the dehydrated phase not only changes the microstructure, it appears to also redistribute the Pb^{2+} ions. CL analysis shows that the PL no longer originates from a few small regions on the nanometer length scale but rather from micron-sized crystallites. In those samples that are heated to 80 °C in solution prior to filtration, no evidence for the presence of Cs_4PbBr_6 or $CsPbBr_3$ can be seen in synchrotron PXRD scans, yet blue PL is seen that is very similar to powdered samples that were heated above the dehydration temperature and cooled back to room temperature. These observations provide strong evidence that the blue PL originates from Pb^{2+} ions that are substituted into $Cs_2InBr_5{\cdot}H_2O$ crystals.

Substitution of Pb^{2+} on an In^{3+} site would presumably be accompanied by charge compensating defects. A bromide vacancy near the Pb^{2+} impurity would charge-balance the dopant site, and in the absence of coordinating H_2O molecules, this would create $[PbBr_4]^{2-}$ complex ions. We hypothesize that these ions are the source of blue emission seen in $Cs_2InBr_5{\cdot}H_2O$ samples that have been heated above the dehydration temperature. The emission profile seen in the blue PL samples studied here is very similar to that of $[PbBr_4]^{2-}$ species found in compounds such as $Bmpip_2PbBr_4$ and $(C_{13}H_{19}N_4)_2PbBr_4$. In both of these compounds, the emission is thought to arise from the $^3P_1 \rightarrow {}^1S_0$ transition of isolated $[PbBr_4]^{2-}$ polyhedra in a disphenoidal (seesaw) configuration.[39,41] The continual red-shift of emission that occurs over time in $Cs_2InBr_5{\cdot}H_2O{:}Pb^{2+}$ samples with blue PL reflects the inherent instability of these aliovalent doping sites.

The synthesis of perovskite NCs has been widely studied, and routes to stable nanoparticles are of great interest. The $Cs_2InBr_5{\cdot}H_2O{:}Pb^{2+}$ system affords a greener synthesis route to perovskite NCs compared to Cs_4PbBr_6 which requires organic solvents such as DMSO or DMF. Unlike phase-pure $CsPbBr_3$ NC, emission from these NCs embedded in a $Cs_2InBr_5{\cdot}H_2O$ matrix are stable when exposed to ambient conditions. Although Pb^{2+} is still present in this material, its concentration is much reduced compared to $CsPbBr_3$ NC embedded in a Cs_4PbBr_6 host where lead is an intrinsic part of the structure. Furthermore, the emission characteristics can be transformed by mild heat treatment to a strong blue emission with moderately high quantum yield (41%). While the blue emitting samples are not as stable upon exposure to ambient atmospheres as the green emitting samples, this work shows that the Pb^{2+} ion is a viable activator in metal halide phosphors and luminescent materials.

CONCLUSIONS

$Cs_2InBr_5{\cdot}H_2O$ samples prepared via precipitation from HBr(aq) solutions in the presence of Pb^{2+} exhibit narrowband green PL. Synchrotron PXRD, optical properties, and CL imaging analysis indicate that the emission originates in $CsPbBr_3$ NC. Unlike pure $CsPbBr_3$ NC, these samples and their PL are stable indefinitely upon exposure to ambient atmosphere. Upon heating to 80 °C, samples can be converted from green emitting to blue emitting powders. This is triggered by a dehydration and subsequent rehydration of the $Cs_2InBr_5{\cdot}H_2O$ structure, resulting in grain growth and partial dissolution of Cs_4PbBr_6 and/or $CsPbBr_3$ inclusions leading to a more uniform dispersion Pb^{2+} ions. PL in blue emitting samples appears to originate from isolated Pb^{2+} ions that substitute on In^{3+} sites of the host structure.

ASSOCIATED CONTENT

Supporting Information

The Supporting Information is available free of charge at https://pubs.acs.org/doi/10.1021/acs.chemmater.2c02817.

Laboratory and synchrotron PXRD data; Scherrer analysis used to estimate the domain size of $CsPbBr_3$ crystallites; Tauc plot and emission spectrum for a green emitting $Cs_2InBr_5{\cdot}H_2O$; PLQY analysis; UV−vis diffuse reflectance spectra, emission spectra, and excitation spectra of green emitting $Cs_2InBr_5{\cdot}H_2O{:}Pb^{2+}$ and Cs_4PbBr_6; emission spectrum for a blue emitting $Cs_2InBr_5{\cdot}H_2O$ sample; refined lattice parameters of

https://doi.org/10.1021/acs.chemmater.2c02817
Chem. Mater. 2023, 35, 482−489

various samples; CIE coordinates for various luminescence; CL images of both green and blue emitting $Cs_2InBr_5{\cdot}H_2O{:}Pb^{2+}$ as well as orange emitting $Cs_2InBr_5{\cdot}H_2O{:}Sb^{3+}$ (PDF)

AUTHOR INFORMATION

Corresponding Author

Patrick M. Woodward − *Department of Chemistry and Biochemistry, The Ohio State University, Columbus, Ohio 43210, United States;* orcid.org/0000-0002-3441-2148; Email: woodward.55@osu.edu

Authors

Jackson D. Majher − *Department of Chemistry and Biochemistry, The Ohio State University, Columbus, Ohio 43210, United States;* orcid.org/0000-0002-4160-4201

Victor da Cruz Pinha Barbosa − *Department of Chemistry and Biochemistry, The Ohio State University, Columbus, Ohio 43210, United States*

Chris Chae − *Department of Materials Science and Engineering, The Ohio State University, Columbus, Ohio 43210, United States*

T. Amanda Strom − *Department of Material Science, UC Santa Barbara, Santa Barbara, California 93106, United States*

Jinwoo Hwang − *Department of Materials Science and Engineering, The Ohio State University, Columbus, Ohio 43210, United States*

Complete contact information is available at: https://pubs.acs.org/10.1021/acs.chemmater.2c02817

Author Contributions

J.D.M. conceived this study and carried out all of the synthesis and characterization except as noted below. V.d.C.P.B. performed the TGA. T.A.S. performed the PLQY measurements. C.C. and J.H. performed the SEM and CL measurements. J.D.M. and P.M.W. interpreted the results and took the lead in writing the manuscript, which was completed through contributions of all authors. All authors have given approval to the final version of the manuscript.

Notes

The authors declare no competing financial interest.

ACKNOWLEDGMENTS

The authors would like to acknowledge Matthew Gray for helpful discussions while composing the manuscript. Funding was provided by the National Science Foundation under award number DMR-2003793. Chae and Hwang acknowledge support by National Science Foundation, DMR-2011876. The MRL Shared Experimental Facilities are supported by the MRSEC Program of the NSF under Award no. DMR-1720256; a member of the NSF-funded Materials Research Facilities Network (www.mrfn.org). Use of the APS at Argonne National Laboratory was supported by the U. S. Department of Energy, Office of Science, Office of Basic Energy Sciences, under Contract no. DE-AC02-06CH11357.

REFERENCES

(1) Jena, A. K.; Kulkarni, A.; Miyasaka, T. Halide Perovskite Photovoltaics: Background, Status, and Future Prospects. *Chem. Rev.* **2019**, *119*, 3036−3103.

(2) Kim, J. Y.; Lee, J.; Jung, H.; Shin, H.; Park, N. High-Efficiency Perovskite Solar Cells. *Chem. Rev.* **2020**, *120*, 7867−7918.

(3) Kang, J.; Wang, L. High Defect Tolerance in Lead Halide Perovskite $CsPbBr_3$. *J. Phys. Chem. Lett.* **2017**, *8*, 489−493.

(4) Shamsi, J.; Urban, A. S.; Imran, M.; De Trizio, L. D.; Manna, L. Metal Halide Perovskite Nanocrystals: Synthesis, Post-Synthesis Modifications, and Their Optical Properties. *Chem. Rev.* **2019**, *119*, 3296−3348.

(5) Schmidt, L. C.; Pertegás, A.; González-Carrero, S.; Malinkiewicz, O.; Agouram, S.; Espallargas, G. M. M.; Bolink, R. E.; Galian, J.; Pérez-Prieto, J. Nontemplate Synthesis of $CH_3NH_3PbBr_3$ Perovskite Nanoparticles. *J. Am. Chem. Soc.* **2014**, *136*, 850−853.

(6) Nedelcu, G.; Protesescu, L.; Yakunin, S.; Bodnarchuk, M. I.; Grotevent, M. J.; Kovalenko, M. V. Fast Anion-Exchange in Highly Luminescent Nanocrystals of Cesium Lead Halide Perovskites ($CsPbX_3$, X = Cl, Br, I). *Nano Lett.* **2015**, *15*, 5635−5640.

(7) Lin, K.; Xing, J.; Quan, L. N.; de Arquer, P. G.; Gong, X.; Lu, J.; Xie, L.; Zhao, W.; Zhang, D.; Yan, C.; Li, W.; Liu, X.; Lu, Y.; Kirman, J.; Sargent, E. H.; Xiong, W.; Wei, Z. Perovskite light-emitting diodes with external quantum efficiency exceeding 20 per cent. *Nature* **2018**, *562*, 245−248.

(8) Chen, Q.; Wu, J.; Ou, X.; Huang, B.; Almutlaq, J.; Zhumekenov, A. A.; Guan, X.; Han, S.; Liang, L.; Yi, Z.; et al. All-inorganic perovskite nanocrystal scintillators. *Nature* **2018**, *561*, 88−93.

(9) Zhu, H.; Fu, Y.; Meng, F.; Wu, X.; Gong, Z.; Ding, Q.; Gustafsson, M. V.; Trinh, M. T.; Jin, S.; Zhu, X.-Y. Lead halide perovskite nanowire lasers with low lasing thresholds and high quality factors. *Nat. Mater.* **2015**, *14*, 636−642.

(10) Ricci, F.; Marougail, V.; Varnavski, O.; Wu, Y.; Padgaonkar, S.; Irgen-Gioro, S.; Weiss, S.; Goodson, E. A.; Goodson, T., III Enhanced Exciton Quantum Coherence in Single $CsPbBr_3$ Perovskite Quantum Dots using Femtosecond Two-Photon Near-Field Scanning Optical Microscopy. *ACS Nano* **2021**, *15*, 12955−12965.

(11) McClure, E. T.; Ball, M. R.; Windl, W.; Woodward, P. M. Cs_2AgBiX_6 (X = Br, Cl): New Visible Light Absorbing, Lead-Free Halide Perovskite Semiconductors. *Chem. Mater.* **2016**, *28*, 1348−1354.

(12) Volonakis, G.; Haghighirad, A. A.; Milot, R. L.; Sio, W. H.; Filip, M. R.; Wenger, B.; Johnston, M. B.; Herz, L. M.; Snaith, H. J. $Cs_2InAgCl_6$: A New Lead-Free Halide Perovskite with Direct Band Gap. *J. Phys. Chem. Lett.* **2017**, *8*, 722−778.

(13) Wu, Y.; Li, X.; Zeng, H. Lead-Free Halide Double Perovskites: Structure, Luminescence, and Applications. *Small Struct.* **2021**, *2*, 20000071.

(14) Majher, J. D.; Gray, M. B.; Strom, T. A.; Woodward, P. M. $Cs_2NaBiCl_6{:}Mn^{2+}$−A New Orange-Red Halide Double Perovskite Phosphor. *Chem. Mater.* **2019**, *31*, 1738−1744.

(15) Zhao, F.; Song, Z.; Zhao, J.; Liu, Q. Double perovskite $Cs_2AgInCl_6{:}Cr^{3+}$: broadband and near-infrared luminescent materials. *Inorg. Chem. Front.* **2019**, *6*, 3621−3628.

(16) Li, S.; Hu, Q.; Luo, J.; Jin, T.; Liu, J.; Li, J.; Tan, Z.; Han, Y.; Zheng, Z.; Zhai, T.; et al. Self-trapped Exciton to Dopant Energy Transfer in Rare Earth Doped Lead-Free Double Perovskite. *Adv. Opt. Mater.* **2019**, *7*, 1901098.

(17) Liu, Y.; Rong, X.; Li, M.; Molokeev, M.; Zhao, J.; Xia, Z. Incorporating Rare-Earth Terbium(III) Ions into $Cs_2AgInCl_6$:Bi Nanocrystals toward Tunable Photoluminescence. *Angew. Chem., Int. Ed.* **2020**, *59*, 11634−11640.

(18) Luo, J.; Wang, X.; Li, S.; Liu, J.; Guo, Y.; Niu, G.; Yao, L.; Fu, Y.; Gao, L.; Dong, Q.; et al. Efficient and stable emission of warm-white light from lead-free halide double perovskites. *Nature* **2018**, *563*, 541−545.

(19) Gray, M. B.; Hariyani, S.; Strom, T. A.; Majher, J. D.; Brgoch, J.; Woodward, P. M. High-efficiency blue photoluminescence in the $Cs_2NaInCl_6{:}Sb^{3+}$ double perovskite phosphor. *J. Mater. Chem. C* **2020**, *8*, 6797−6803.

(20) Zeng, R.; Zhang, L.; Xue, Y.; Ke, B.; Zhao, Z.; Huang, D.; Wei, Q.; Zhou, W.; Zou, B. Highly Efficient Blue Emission from Self-

Trapped Excitons in Stable Sb^{3+}-Doped $Cs_2NaInCl_6$ Double Perovskites. *J. Phys. Chem. Lett.* **2020**, *11*, 2053−2061.
(21) Noculak, A.; Morad, V.; McCall, K. M.; Yakunin, S.; Shynkarenko, Y.; Wörle, M.; Kovalenko, M. V. Bright Blue and Green Luminescence of Sb(III) in Double Perovskite Cs_2MInCl_6 (M = Na, K) Matrices. *Chem. Mater.* **2020**, *32*, 5118−5124.
(22) Arfin, H.; Kshirsagar, A. S.; Kaur, J.; Mondal, B.; Xia, Z.; Chakraborty, S.; Nag, A. ns^2 Electron (Bi^{3+} and Sb^{3+}) Doping in Lead-Free Metal Halide Perovskite Derivatives. *Chem. Mater.* **2020**, *32*, 10255−10267.
(23) Tan, Z.; Li, J.; Zhang, C.; Li, Z.; Hu, Q.; Xiao, Z.; Kamiya, T.; Hosono, H.; Niu, G.; Lifshitz, E.; Cheng, Y.; Tang, J. Highly Efficient Blue-Emitting Bi-Doped Cs_2SnCl_6 Perovskite Variant: Photoluminescence Induced by Impurity Doping. *Adv. Funct. Mater.* **2018**, *28*, 1801131.
(24) Li, J.; Tan, Z.; Hu, M.; Chen, C.; Luo, J.; Li, S.; Gao, L.; Xiao, Z.; Niu, G.; Tang, J. Antimony doped Cs_2SnCl_6 with bright and stable emission. *Front. Optoelectron.* **2019**, *12*, 352−364.
(25) Zeng, R.; Bai, K.; Wei, Q.; Chang, T.; Yan, J.; Ke, B.; Huang, J.; Wang, L.; Zhou, W.; Cao, S.; Zhao, J.; Zou, B. Boosting triplet self-trapped exciton emission in Te(IV)-doped Cs_2SnCl_6 perovskite variants. *Nano Res.* **2021**, *14*, 1551−1558.
(26) Jing, Y.; Liu, Y.; Zhao, J.; Xia, Z. Sb^{3+} Doping-Induced Triplet Self-Trapped Excitons Emission in Lead-Free Cs_2SnCl_6 Nanocrystals. *J. Phys. Chem. Lett.* **2019**, *10*, 7439−7444.
(27) Majher, J. D.; Gray, M. B.; Liu, T.; Holzapfel, N. P.; Woodward, P. M. Rb_3InCl_6: A Monoclinic Double Perovskite Derivative with Bright Sb^{3+}-Activated Photoluminescence. *Inorg. Chem.* **2020**, *59*, 14478−14485.
(28) Zhu, D.; Zaffalon, M. L.; Zito, J.; Cova, F.; Meinardi, F.; De Trizio, L. D.; Infante, I.; Brovelli, S.; Manna, L. Sb-Doped Metal Halide Nanocrystals: A 0D versus 3D Comparison. *ACS Energy Lett.* **2021**, *6*, 2283−2292.
(29) Jing, Y.; Liu, Y.; Jiang, X.; Molokeev, M. S.; Lin, Z.; Xia, Z. Sb^{3+} Dopant and Halogen Substitution Triggered Highly Efficient and Tunable Emission in Lead-Free Metal Halide Single Crystals. *Chem. Mater.* **2020**, *32*, 5327−5334.
(30) Liu, X.; Xu, X.; Li, B.; Liang, Y.; Li, Q.; Jiang, H.; Xu, D. Antimony-Doping Induced Highly Efficient Warm-White Emission in Indium-Based Zero-Dimensional Perovskites. *CCS Chem.* **2020**, *2*, 216−224.
(31) Zhou, L.; Liao, J.; Huang, Z.; Wei, J.; Wang, X.; Li, W.; Chen, H.; Kuang, D.; Su, C. A Highly Red-Emissive Lead-Free Indium-Based Perovskite Single Crystal for Sensitive Water Detection. *Angew. Chem., Int. Ed.* **2019**, *58*, 5277−5281.
(32) Saidaminov, M. I.; Almutlaq, J.; Sarmah, S.; Dursun, I.; Zhumekenov, A. A.; Begum, R.; Pan, J.; Cho, N.; Mohammed, O. F.; Bakr, O. M. Pure Cs_4PbBr_6: Highly Luminescent Zero-Dimensional Perovskite Solids. *ACS Energy Lett.* **2016**, *1*, 840−845.
(33) Quan, L.; Quintero-Bermudez, R.; Voznyy, O.; Walters, G.; Jain, A.; Fan, J. Z.; Zheng, X.; Yang, Z.; Sargent, E. H. Highly Emissive Green Perovskite Nanocrystals in a Solid-State Crystalline Matrix. *Adv. Mater.* **2017**, *29*, 16059.
(34) Topas Academic. *General Profile and Structural Analysis for Powder Diffraction Data*; Bruker AXS: Karlsruhe: Germany, 2004.
(35) Momma, K.; Izumi, F. VESTA 3 for three−dimensional visualization of crystal, volumetric and morphology data. *J. Appl. Crystallogr.* **2011**, *44*, 1272−1276.
(36) Chen, Y.; Zhou, Y.; Zhao, Q.; Zhang, J.; Ma, J.; Xuan, T.; Guo, S.; Yong, Z.; Wang, J.; Kuroiwa, Y.; Moriyoshi, C.; Sun, H. Cs_4PbBr_6/$CsPbBr_3$ Perovskite Composites with Near-Unity Luminescence Quantum Yield: Large-Scale Synthesis, Luminescence and Formation Mechanism, and White-Light-Emitting Diode Application. *ACS Appl. Mater. Interfaces* **2018**, *10*, 15905−15912.
(37) Nedulcu, G.; Protesescu, L.; Yankunin, S.; Bodnarchuk, M. I.; Grotevent, M. J.; Kovalenko, M. V. Fast Anion-Exchange in Highly Luminescent Nanocrystals of Cesium Lead Halide Perovskites ($CsPbX_3$, X = Cl, Br, I). *Nano Lett.* **2015**, *15*, 5635−5640.
(38) Riesen, N.; Lockrey, M.; Badek, K.; Riesen, H. On the origins of the green luminescence in the "zero-dimensional perovskite" Cs_4PbBr_6: conclusive results from cathodoluminescence imaging. *Nanoscale* **2019**, *11*, 3925−3932.
(39) Morad, V.; Shynkarenko, Y.; Yakunin, S.; Brumberg, A.; Schaller, R. D.; Kovalenko, M. V. Disphenoidal Zero-Dimensional Lead, Tin, and Germanium Halides: Highly Emissive Singlet and Triplet Self-Trapped Excitons and X-ray Scintillation. *J. Am. Chem. Soc.* **2019**, *141*, 9764−9768.
(40) Kostopoulou, A.; Sygletou, M.; Brintakis, K.; Lappas, A.; Stratakis, E. Low-temperature benchtop-synthesis of all-inorganic perovskite nanowires. *Nanoscale* **2017**, *9*, 18202−18207.
(41) Lin, H.; Zhou, C.; Chaaban, M.; Xu, L.; Zhou, Y.; Neu, J.; Worku, M.; Berkwits, E.; He, Q.; Lee, S.; Tin, X.; Siegrist, T.; Du, M.; Ma, B. Bulk Assembly of Zero-Dimensional Organic Lead Bromide Hybrid with Efficient Blue Emission. *ACS Mater. Lett.* **2019**, *1*, 594−598.

https://doi.org/10.1021/acs.chemmater.2c02817
Chem. Mater. 2023, 35, 482−489